ARTICLE

Effective Variables To Control the Fill Factor of Organic Photovoltaic Cells

Myung-Su Kim,[†] Bong-Gi Kim,[‡] and Jinsang Kim*[,†,‡,§]

Departments of Materials Science and Engineering, Macromolecular Science and Engineering, and Chemical Engineering, University of Michigan, Ann Arbor, Michigan 48109

ABSTRACT Effective cell design variables having a large impact on the fill factor (FF) of organic photovoltaic cells (OPVCs) were systematically identified using a general device structure of ITO/PEDOT:PSS/P3HT + PCBM/LiF/Al. The results show that the characteristic properties of the organic layer, such as morphology and thickness, the regioregularity of the conjugated polymer, and the two interfaces between the electrodes and the blend layer have a large influence on the FF by affecting the series resistance (R_s) and the shunt resistance (R_{sh}). The systematic investigation described in this contribution provides a comprehensive understanding of the correlation between the device variables and R_s and R_{sh} and a way to control FF, which is critically important to achieving a high-performance OPVC.

KEYWORDS: organic photovoltaic cells • fill factor • series resistance • shunt resistance • cell design parameters

INTRODUCTION

Organic photovoltaic cells (OPVCs) have attracted much interest as ecofriendly energy-converting devices. The power conversion efficiency (PCE) of OPVC has been improved rapidly and is currently in the range of 3.5−6.5% (1−5). The best PCE of a single-cell OPVC is about 5%, which was achieved from the cells composed of poly(3-hexylthiophene) (P3HT) and phenyl-C61-butyric acid methyl ester (PCBM) even though a tandem cell having 6.5% PCE was recently reported (1). Considering that a minimum of 10% PCE is required for the practical application of photovoltaic technology, much more progress is demanded. Among the crucial limiting factors of the PCE of OPVC are the limited light absorption efficiency, the short exciton diffusion length, and the low hole mobility ($\sim 10^{-3}$ $cm^2/V \cdot s$) in the semiconducting organic layer (6, 7). To overcome these limits, much effort has been made including tandem cell design, new material development, control of the molecular packing and morphology of the semiconducting layer, and the design of nanostructures (1, 8−10).

A thorough understanding of the parameters that affect the short-circuit current density (J_{sc}), open-circuit voltage (V_{oc}), and fill factor (FF) is critically important to optimizing the PCE of OPVC. FF is defined as $J_{max}V_{max}/J_{sc}V_{oc}$ and shown in Figure 1a. Gupta et al. investigated the concave down-shaped or S-like *JV* curve that causes a drastically small FF (11). In their investigation, the concave down-shaped *JV* curve was explained to be formed by charge accumulation at the interface between the electrode and the organic semiconducting layer. To verify that hypothesis, the authors prepared two types of OPVCs. The first one was indium−tin oxide (ITO)/poly(3,4-ethylenedioxythiophene) with poly(styrenesulfonate) (PEDOT:PSS)/P3HT + PCBM/Al, and the other was ITO/PEDOT:PSS/P3HT + PCBM/Ca/Al. The former device showed the concave down-shaped *IV* curve, and the obtained FF was only 0.12. In the latter device, the additional thin calcium layer at the interface between the aluminum cathode and the organic layer facilitates charge collection because of the ohmic contact, and the resulting FF was improved by up to 0.37. Instead of calcium, Brabec et al. added a lithium fluoride (LiF) layer between the aluminum cathode and the semiconducting blend layer and observed an enhanced FF from 0.5 to 0.6 (12). In this case, the authors attributed the enhanced FF to the dipole formation induced by LiF rather than the ohmic contact formation.

In this contribution, we report our investigation on the relationships between the FF and various cell design parameters. The general device structure was ITO/PEDOT:PSS/P3HT + PCBM/LiF/Al. We used the island-type electrode geometry to prevent the additional charge collection observed from the crossbar-type device configuration (14). We systematically investigated the effects of the characteristic properties of the organic layer to the FF, such as morphology and thickness, the regioregularity of the conjugated polymer, and the two interfaces between the electrodes and the blend layer.

EXPERIMENTAL SECTION

Materials. In this investigation, two isomeric conjugated polymers were used; the regiorandom poly(3-hexylthiophene) (P3HT) was polymerized by using $FeCl_3$, and the regioregular P3HT was purchased from Rieke Metals. Phenyl-C61-butyric acid methyl ester (PCBM) was purchased from American Dye source.

Device Fabrication and Characterization. ITO-coated glasses were cleaned with acetone and isopropyl alcohol. After the substrates were dried with air, they were treated with UV ozone

* To whom correspondence should be addressed. E-mail: jinsang@umich.edu.
Received for review March 9, 2009 and accepted May 13, 2009
[†] Department of Materials Science and Engineering.
[‡] Department of Macromolecular Science and Engineering.
[§] Department of Chemical Engineering.
DOI: 10.1021/am900155y

Published on Web 05/28/2009

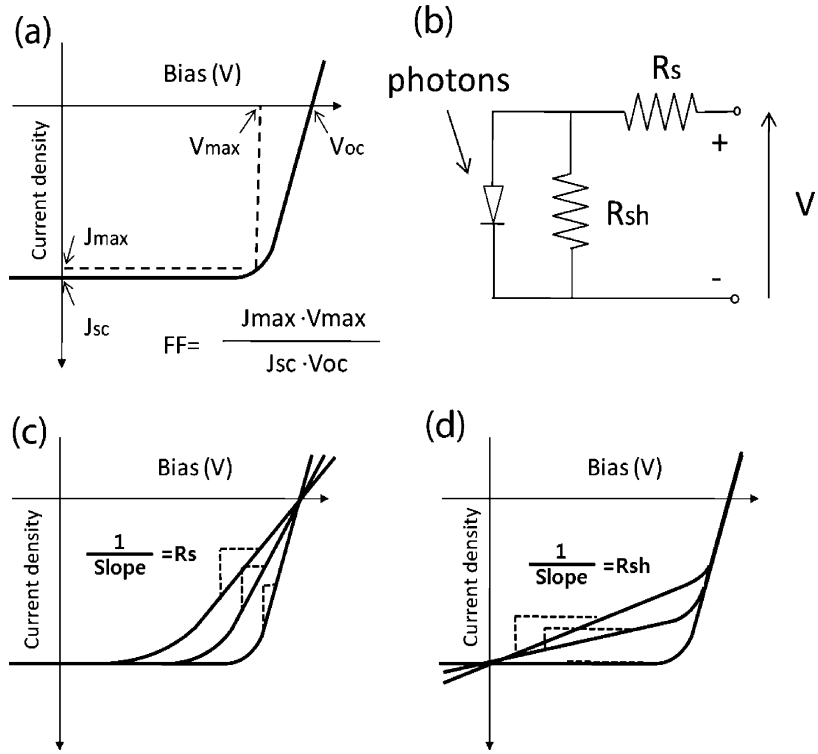

FIGURE 1. (a) Definition of FF. J_{max} = current density at the maximum of JV in the fourth quadrant, and V_{max} = bias at the maximum of JV in the fourth quadrant. (b) Circuit model of a photovoltaic device. R_s = series resistance, and R_{sh} = shunt resistance. (c) Impact of the variation of the series resistance (R_s) on the FF. The indicated inverse slope represents R_s. (d) Impact of the variation of the shunt resistance (R_{sh}) on the FF. The indicated inverse slope represents R_{sh} (13).

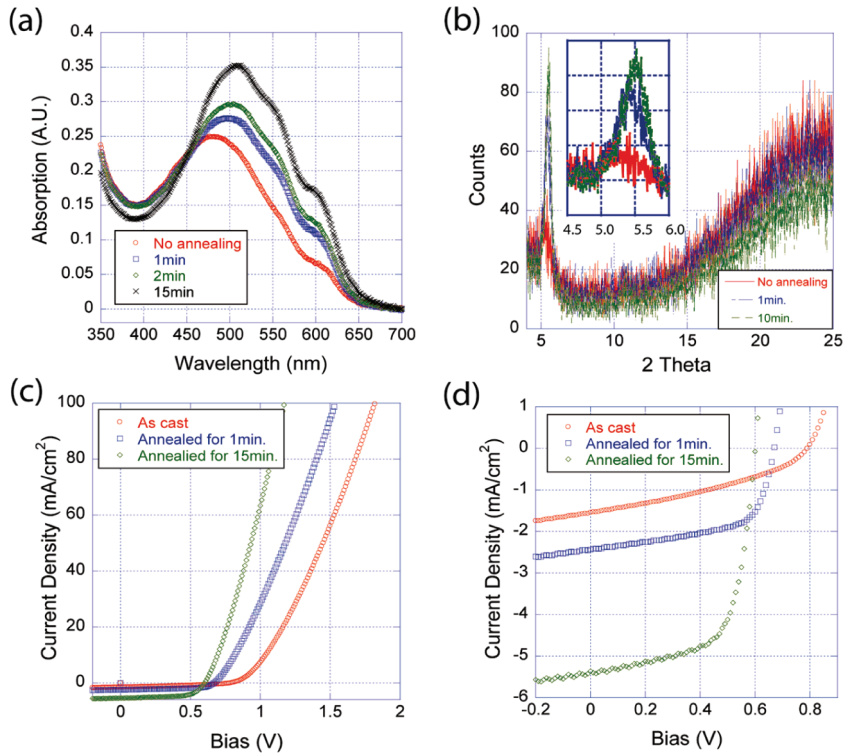

FIGURE 2. Annealing effect on the FF of OPVCs: (a) effect of thermal annealing on the absorption property; (b) XRD data showing the effect of thermal annealing on the crystallinity of P3HT; (c and d) Effect of thermal annealing on the $J-V$ curve at different scales.

for 5 min. PEDOT:PSS (Baytron PH 500) was spin-cast on the cleaned ITO as received and baked at 130 °C for 15 min. To vary the conductivity of PEDOT:PSS, 5 wt % dimethyl sulfoxide (DMS) was added in a PEDOT:PSS solution. The blend solutions of the conjugated polymers and PCBM (1:1 wt %, 20 mg/mL in chlorobenzene) were prepared by stirring of the solution for 24 h in a glovebox and spin-cast at 1000 rpm for 30 s. The samples were then annealed at 130 °C. Layers of 1 nm of LiF and 100 nm of Al were deposited sequentially at 5×10^{-7} Torr. When only Al was deposited without LiF, the devices were

Table 1. Performances of P3HT and PCBM Blend Photovoltaic Devices under Various Annealing Conditions

annealing time (min)	J_{sc}(mA/cm^2)	V_{oc}(V)	PCE (%)	R_s(Ω cm^2)	FF
0	1.54	0.8	0.44	6.99	0.36
1	2.43	0.67	0.99	6.19	0.61
15	5.36	0.6	2.10	3.65	0.65

Table 2. Device Performances of the Photovoltaic Cells Having Regioregular P3HT/PCBM and Regiorandom P3HT/PCBM

	J_{sc} (mA/cm^2)	V_{oc} (V)	PCE (%)	FF	R_s (Ω cm^2)	R_{sh} (Ω cm^2)
regiorandom P3HT + PCBM	0.65	0.59	0.12	0.31	13	900
regioregular P3HT + PCBM	5.40	0.60	2.12	0.65	3.6	1205

annealed after Al deposition. All devices were characterized under ambient conditions, and the typical illumination intensity was 100 mW/cm^2 (AM 1.5G Oriel solar simulator). For investigation of the illumination intensity effect on FF, the illumination intensity was controlled from 10 to 1000 mW/cm^2. The $J-V$ plots were recorded using a HP semiconductor analyzer. The R_s and R_{sh} values were calculated from the inverse slope of the $J-V$ curve in the fourth quadrant, as illustrated in Figure 1c,d (15).

X-ray diffraction (XRD). The P3HT:PCBM blend solution was spin-cast onto a glass substrate at 1000 rpm for 30 s. Three spin-cast samples were annealed for 0, 1, and 10 min, respectively. XRD patterns were collected on a Rigaku diffractometer by using Cu KR radiation from a Rigaku 12 kW rotating-anode X-ray generator.

RESULTS AND DISCUSSION

FF is determined by the series resistance (R_s) and the shunt resistance (R_{sh}) of the device, as illustrated in Figure 1c,d (13, 15). The series resistance, R_s, can be calculated from the inverse slope of the $J-V$ curve in the first quadrant (Figure 1c) and is closely related with the intrinsic resistance, morphology, and thickness of the semiconductor layer. On the other hand, the shunt resistance R_{sh} is correlated with the amount and character of the impurities and defects in the active organic semiconductor layer because impurities and defects cause charge recombination and leakage current. R_{sh} determines the inverse slope of the $J-V$ curve in the fourth quadrant, as shown in Figure 1d.

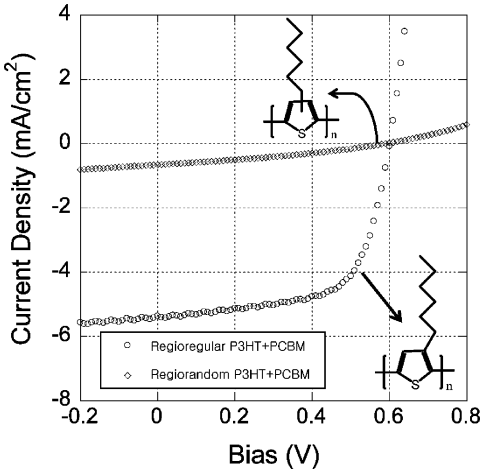

FIGURE 3. Effect of the regioregularity of conjugated polymers on FF.

We first investigated the effect of the blend morphology of the organic semiconducting layer that is composed of regioregular P3HT and PCBM. Regioregular P3HT can form crystalline domains because of the regioregularity. The crystallinity can be controlled by tuning the molecular packing of the polymer through thermal annealing (4). When the blend layer was thermally annealed at 130 °C for 1−15 min, the blend film showed a bathochromic shift to a dark-purple color. As shown in Figure 2a, the bathochromic shift is evident by the gradual shift of the absorption λ_{max} from 500 to 520 nm along with the annealing time. The overall absorption efficiency also increased because of the formation of the ground-state aggregation and the backbone planarization (16−18). The regular molecular packing in the crystalline domains induced by thermal annealing was confirmed by XRD (Figure 2b). The sharp peak at 5.4° corresponds to a 16 Å spacing that is close to the length of the fully extended hexyl side chain of 13 Å. Therefore, this peak can be assigned to the distance between the regioregular P3HT backbones when the hexyl side chains of the regioregular P3HT are interdigitated in the crystal (4). As the sample was annealed, the peak at 5.4° grew, indicating that thermal annealing induced better molecular packing. The broad peak at 25° (3.8 Å spacing) originates from the distance between the cofacially arranged thiophene rings in the crystal.

The molecular packing of the conjugated polymer turns out to be an important parameter affecting R_s of the OPVC (Figure 2c and Table 1). As the device was annealed, R_s decreased from 6.99 to 3.65 Ω cm^2 because thermally induced enhanced intermolecular packing and crystallization allow more efficient intra- and intermolecular charge transport through the conjugated polymer in the blend layer (19). Kinks and torsional disorder along the conjugated polymer backbone can be considered defects that increase the resistivity of the conjugated polymer as a conducting conduit (20). Because the conjugated polymers pack densely through thermal annealing, kinks and torsional disorder should be reduced to some extent. Furthermore, densely packed conjugated polymer backbones will provide more efficient intermolecular charge hopping as well.

The detailed device performances are summarized in Table 1. As the active layer was annealed, the PCE increased from 0.44% to 2.10% mainly because of the increased J_{sc} and FF. The increase in FF from 0.36 to 0.65 originates from the reduced R_s by thermal annealing. However, R_{sh} did not change with thermal annealing. The $J-V$ curves in Figure 2d show essentially the same R_{sh} values. The enhanced J_{sc} can be attributed to not only the increased absorption efficiency but also the reduced resistivity of the blend layer.

As a supporting experiment for the molecular packing consideration, we built photovoltaic cells with regiorandom

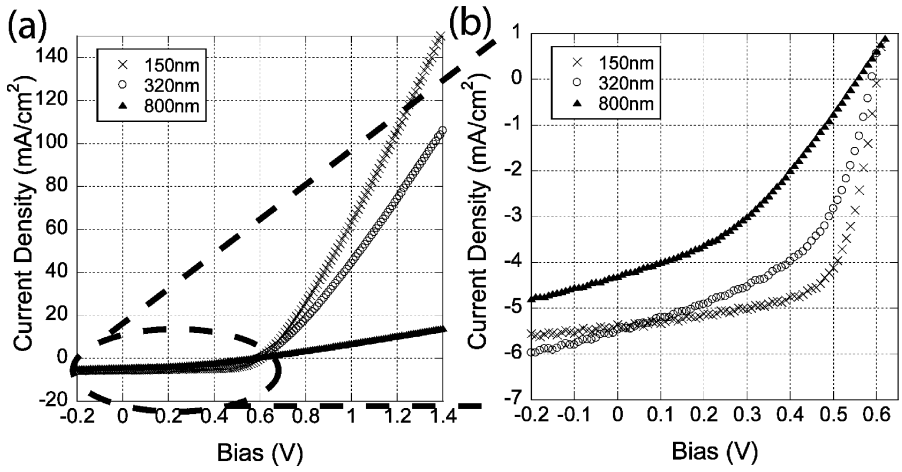

FIGURE 4. Thickness effect on FF.

Table 3. Device Performance Depending on the Blend Layer Thickness Effect

P3HT/PCBM layer thickness (nm)	J_{sc} (mA/cm^2)	V_{oc} (V)	PCE (%)	R_s (Ω cm^2)	R_{sh} (Ω cm^2)	FF
150	5.36	0.60	2.10	3.7	909	0.65
320	5.47	0.58	1.62	6.0	319	0.51
800	4.31	0.55	0.91	52.0	229	0.38

P3HT and examined the effect of the regioregularity on FF. All other fabrication conditions were kept the same. Even after the same thermal annealing, the cells having regiorandom P3HT did not show any color change, unlike the regioregular P3HT, because of the lack of molecular regularity required for crystallization. As we can clearly see from Figure 3, the performance of the cells composed of the regioregular P3HT was much better than that of the cells with the regiorandom P3HT. R_s of the regioregular P3HT cells was 1 order of magnitude smaller than that of the regiorandom P3HT cells, while J_{sc} of the regioregular P3HT cells was 1 order of magnitude larger than that of the regiorandom P3HT cells. The regioregularity has a minor effect on R_{sh}. As one can see from the slopes of the $J-V$ curves in the fourth quadrant, there is no large change in R_{sh}. Because of the smaller R_s, the FF of the regioregular P3HT cells was much larger (0.65) than that of the regiorandom cells (0.31). These data clearly support that the morphology and molecular packing of the blend layer are determinant of FF.

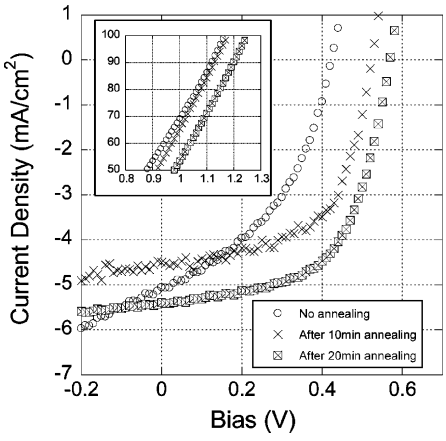

FIGURE 5. Effect of the interface between the cathode and the blend layer. (Inset) $J-V$ curves from 0.8 to 1.3 V showing R_s.

Table 4. Effects of the Interface between the Cathode and the Blend Layer on the FF

	J_{sc} (mA/cm^2)	V_{oc} (V)	PCE (%)	FF	R_{sh} (Ω cm^2)
not annealed	5.06	0.42	0.92	0.43	149
annealed for 10 min	4.50	0.52	1.37	0.59	533
annealed for 20 min	5.40	0.56	1.81	0.60	676

Another important variable in the blend layer having an impact on FF is the film thickness of the organic semiconducting layer. We varied the thickness of the P3HT/PCBM layer from 150 to 800 nm and found increased R_s and decreased R_{sh} as the device thickness was increased. The obtained $J-V$ curves shown in Figure 4a,b and Table 3 clearly demonstrate the relationship between the device thickness and R_s and R_{sh}. As the device thickness was increased, R_s increased from 3.7 to 52 Ω cm^2, indicating that the blend layer became more resistive and R_{sh} decreased from 909 to 229 Ω cm^2, implying that there are more charge recombination and leakage current. As a result, FF gradually decreased from 0.65 for the 150-nm-thick cells to 0.38 for the 800-nm-thick cells (16). An interesting phenomenon was observed in Figure 4b. Even though the thickness of the blend layer increased largely from 150 to 320 to 800 nm, J_{sc} minimally increased from the 150 nm cell to the 320 nm cell and even decreased when the thickness was increased further to 800 nm. As the thickness of the energy-harvesting blend layer is increased, more photons should be absorbed into the solar cells. However, the reduced J_{sc} implies that there is more charge recombination in the thicker cells because of the longer travel distance the charges should make to reach the electrodes.

In the previous sections, we showed how the blend layer morphology, regioregularity, and thickness have a significant impact on FF. We further investigated the effects of the two interfaces between the electrodes and the blend layer on FF. First, after Al electrode deposition, the effect of the interface between the cathode and the blend layer was examined before and after thermal annealing. The device structure for this study was ITO/PEDOT:PSS/P3HT + PCBM/Al without

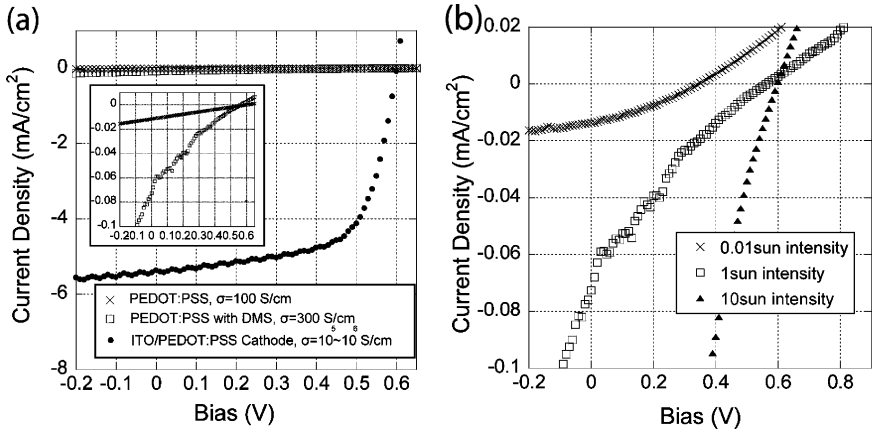

FIGURE 6. (a) Effect of the anode conductivity on FF. (b) Effect of the illumination intensity on FF.

Table 5. Device Performances Depending on the Anode Conductivity

	J_{sc} (mA/cm^2)	V_{oc} (V)	FF
PEDOT:PSS (100 S/cm)	0.02	0.59	0.16
PEDOT:PSS (5 wt % DMS) (300 S/cm)	0.08	0.57	0.20
ITO/PEDOT:PSS (10^5−10^6 S/cm)	5.36	0.60	0.64

Table 6. Performances of the PEDOT:PSS/5 wt % DMS/P3HT + PCBM/LiF/Al Cell Depending on the Illumination Intensity

intensity (sun)	J_{sc} (mA/cm^2)	V_{oc} (V)	FF
0.01	0.01	0.35	0.30
1	0.08	0.57	0.20
10	0.53	0.59	0.17

Table 7. Device Performance of the P3HT/PCBM Photovoltaic Cells under Various Illumination Intensities

intensity (sun)	J_{sc}(mA/cm^2)	V_{oc}(V)	PCE	FF	R_{sh} (Ω cm^2)
0.2	1.64	0.57	2.84	0.61	1825
1	5.83	0.61	2.00	0.56	444
2	11.5	0.64	1.76	0.48	228
3	18.2	0.66	1.63	0.41	136
5	35.5	0.68	1.62	0.34	33

LiF. In order to exclude any morphological effects of the P3HT:PCBM blend layer, before Al electrode deposition, the blend layer was preannealed. Overall, as the device was thermally annealed, all important parameters, J_{sc}, V_{oc} and FF, changed greatly: J_{sc} = 4.5−5.4 mA/cm^2, V_{oc} = 0.42−0.56 V, and FF = 0.43−0.60 (Figure 5 and Table 4). As the device was annealed for up to 20 min, FF changed from 0.43 to 0.60, which can be explained not by R_s but by R_{sh}. The inset of Figure 5 shows a consistent R_s value regardless of the annealing condition. However, R_{sh} increased significantly from 149 to 676 Ω cm^2 when the device was annealed for 20 min. This indicates that annealing reduces charge recombination and leakage current. We believe that thermal annealing induced better Al contact with the blend layer and facilitated charge collection. This is also supported by the improved J_{sc} (4).

The effect of the other interface between the anode and the blend layer was investigated by means of altering the conductivity of the anode from σ = 100 S/cm (PEDOT:PSS, Baytron PH 500) to 300 S/cm (PEDOT:PSS, Baytron PH 500 + 5 wt % DMS) to 10^5−10^6 S/cm (PEDOT:PSS, Baytron PH 500 on ITO). The device structure was anode/P3HT + PCBM/LiF/Al. As we can see in Figure 6a and Table 5, as the anode conductivity was decreased, J_{sc} and FF decreased, implying that the efficiency of the charge extraction through the anode material decreases as the conductivity of the anode decreases (21). To support this hypothesis, we conducted two additional experiments. In the first supporting experiment, the amount of photogenerated charges was controlled by varying the illumination intensity on the cells having PEDOT:PSS + 5 wt % DMS/P3HT + PCBM/LiF/Al (Figure 6b). As the light intensity was decreased from 1 to 0.01 sun intensity, FF increased from 0.20 to 0.30 even though J_{sc} decreased (Figure 6b and Table 6), while when the illumination intensity was increased to 10 sun, FF dropped to 0.17 even though J_{sc} increased. These results support our hypothesis very well.

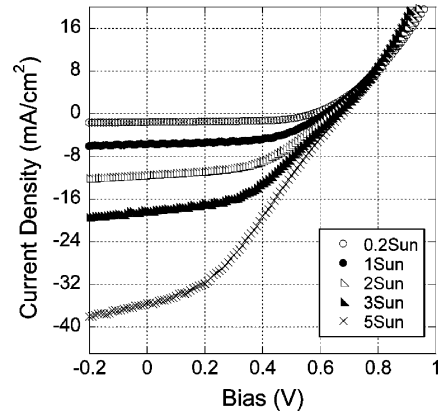

FIGURE 7. J−V curves of the P3HT/PCBM photovoltaic cells under various illumination intensities.

As another supporting experiment, the device having ITO/PEDOT:PSS/P3HT + PCBM/LiF/Al was illuminated with 0.2−5 sun intensity. The resulting J_{sc} increased along with the illumination intensity, while R_{sh} decreased gradually. As the illumination intensity increases, the amount of absorbed photon to the photovoltaic cell will also increase. Therefore, a larger number of photoinduced charges will be generated and result in the increased J_{sc}. However, as the amount of

photoinduced charges increases in the blend layer, the chance of charge recombination can be reasonably expected to increase as well because of the limited charge collection efficiency at the interface between the blend layer and the anode. Therefore, more leakage current will be produced and cause a decrease in R_{sh}. While the illumination intensity largely influences on R_{sh}, it does not affect R_s much, as we can see from Figure 7 and Table 7. Therefore, the inverse correlation between FF and the illumination intensity does not come from R_s but from R_{sh}.

CONCLUSIONS

In summary, in this investigation the effective variables having a large impact on FF of P3HT/PCBM-based OPVC were systematically identified. The results show that the variables in the blend layer component, the blend morphology, the regioregularity of the conjugated polymer, and the thickness of the blend layer have a large influence on FF by affecting R_s and R_{sh}. When the crystallinity of the blend layer was increased by thermal annealing, R_s decreased. When the regioregular P3HT was used, R_s was also reduced by 1 order of magnitude. The higher crystallinity induced by thermal annealing and regioregularity enhances the efficiency of the inter- and intramolecular charge transport. On the contrary, as the thickness of the blend layer was increased, R_s increased and R_{sh} decreased because of the increased distance the charges should travel until they reach the electrodes. This will increase the resistivity and the charge recombination possibility. The quality of the two interfaces between the blend layer and the electrodes was revealed to play a significant role in determining FF as well. When a less conducting cathode was used, FF decreased because of more charge recombination and leakage current that was evidenced by the decrease in R_{sh}. By controlling the amount of the photoinduced charges in the blend layer through various illumination conditions, we could prove that R_{sh} and the resulting FF are largely influenced by the efficiency of the charge extraction through the cathode. As the illumination intensity increased, R_{sh} and FF gradually decreased, indicating that there is more charge recombination in the blend layer. The nature of the interface between the Al anode and the blend layer turns out to be determinant to FF as well. Because the photovoltaic cells were thermally annealed after Al deposition, FF and R_{sh} increased, indicating that the interface became more favorable for charge extraction. It is likely because a better contact is formed between Al and the blend layer by thermal annealing. The systematic investigation described in this contribution provides a comprehensive understanding of the correlation between the device variables and R_s and R_{sh} and the way to control FF, which is critically important to achieving a high-performance OPVC.

Acknowledgment. This work was supported by the NSF (Grant ECCS 0836854) and the Michigan Memorial Phoenix Energy Institute.

REFERENCES AND NOTES

(1) Kim, J. Y.; Lee, K.; Coates, N. E.; Moses, D.; Nguyen, T.-Q.; Dante, M.; Heeger, J. *Science* **2007**, *317*, 222.
(2) Li, G.; Shrotriya, V.; Huang, J.; Yao, Y.; Moriarty, T.; Emery, K.; Yang, Y. *Nat. Mater.* **2005**, *4*, 864.
(3) Kim, Y.; Cook, S.; Tuladhar, S. M.; Choulis, S. A.; Nelsonm, J.; Durrant, J. R.; Bradley, D. C.; Giles, M.; Mcculloch, I.; Ham, C.-S.; Ree, M. *Nat. Mater.* **2006**, *5*, 197.
(4) Ma, W.; Yang, C.; Gong, X.; Lee, K.; Heeger, A. J. *Adv. Funct. Mater.* **2005**, *15*, 1617.
(5) Hoth, C. N.; Schilinsky, P.; Choulis, S. A.; Brabec, C. J. *Nano Lett.* **2008**, *8*, 2806.
(6) Coakley, K. M.; McGehee, M. D. *Chem. Mater.* **2004**, *16*, 4533.
(7) Forrest, S. R. *MRS Bull.* **2005**, *30*, 28.
(8) Kim, M.-S.; Cho, J. C.; Shtein, M.; Guo, L. J.; Kim, J. *Appl. Phys. Lett.* **2007**, *90*, 123113.
(9) Yang, F.; Shtein, M.; Forrest, S. R. *Nat. Mater.* **2005**, *4*, 37.
(10) Williams, S. S.; Hampton, M. J.; Gowrishankar, V.; Ding, K.; Templeton, J. L.; Samulski, E. T.; DeSimone, J. K.; McGehee, M. D. *Chem. Mater.* **2008**, *20*, 5229.
(11) Gupta, D.; Bag, M.; Narayana, K. S. *Appl. Phys. Lett.* **2008**, *92*, 093301.
(12) Brabec, C. J.; Shaheen, S. E.; Winder, C.; Sariciftci, N. S.; Denk, P. *Appl. Phys. Lett.* **2002**, *80*, 1288.
(13) Nelson J. *The physics of solar cells*; Imperial College Press: London, 2002.
(14) Kim, M.-S.; Kang, M.-G.; Guo, L. J.; Kim, J. *Appl. Phys. Lett.* **2008**, *92*, 133301.
(15) So, W.-W.; Moon, S.-J.; Kim, H. *J. Kor. Phys. Soc.* **2006**, *48*, 441.
(16) Shrotriya, V.; Li, G.; Yao, Y.; Yang, Y. *Appl. Phys. Lett.* **2006**, *88*, 073508.
(17) Kim, J.; Swager, T. M. *Nature* **2001**, *411*, 1030.
(18) Kim, J.; Levitsky, I. A.; Swager, T. M. *J. Am. Chem. Soc.* **2002**, *124*, 1446.
(19) Sirringhaus, H.; Brown, P. J.; Friend, R. H.; Nielsen, M. M.; Bechgaard, K.; Langeveld-Voss, B. M. W.; Spiering, A. J. H.; Janssen, R. A. J.; Meijer, E. W.; Herwig, P.; Leeuw, D. M. *Nature* **1999**, *401*, 685.
(20) Grozema, F. C.; van Duijnen, P. Th.; Berlin, Y. A.; Ratner, M. A.; Siebbeles, L. D. A. *J. Phys. Chem. B* **2002**, *106*, 7791.
(21) Zhang, F.; Johansson, M.; Andersson, R.; Hummelen, J. C.; Inganas, O. *Adv. Mater.* **2002**, *14*, 662.

AM900155Y